International Journal of Innovative Computing, Information and Control
Volume **8**, Number **5(A)**, May **2012**

ICIC International ©2012 ISSN 1349-4198
pp. **2965–2977**

GEO SATELLITE AUTONOMOUS NAVIGATION USING X-RAY PULSAR NAVIGATION AND GNSS MEASUREMENTS

Zhi Xiong, Li Qiao, Jianye Liu and Bin Jiang

College of Automation Engineering
Nanjing University of Aeronautics and Astronautics
338 mail box, No. 29, Yudao Street, Baixia District, Nanjing 210016, P. R. China
{xznuaa; qiaoli; ljyac; binjiang}@nuaa.edu.cn

Received December 2010; revised June 2011

Abstract. *Autonomous navigation for High Earth Orbits satellites such as GEO is challenged due to the limitation of the uses of the existing onboard navigation solutions such as GPS/GNSS, celestial navigation. XNAV, Navigation for spaceships using X-ray pulsars shows potential to be the ultimate natural GPS system as an interstellar navigation tool. It indicates that XNAV could assist these to overcome this challenge, an algorithm for satellite autonomous navigation using X-ray navigation and GNSS is presented. X-ray Navigation also known as XNAV is a novel celestial navigation method for aerospace vehicle time, position and attitude determination. X-ray navigation is a GPS-like location technique. GPS/GNSS is demonstrated as an efficient navigation method for GEO. This method utilized an onboard GPS/GNSS receiver to determine the position. The state-of-the-art shows the onboard multi-GNSS will be most likely to be utilized in the earliest real autonomous navigation application. The algorithm is based on a federal Kalman filter and processes X-ray phase measurements and GNSS pseudo-range. Simulation indicates that the integration of X-ray navigation and GNSS achieves position and velocity accuracy better than the performance of single system. Accordingly, the reliability of the entire navigation system can be enhanced through the integration that renders the system especially attractive for future highly autonomous satellite missions.*
Keywords: Autonomous navigation, XNAV, GNSS, Integrated navigation, Federal Kalman filter

1. **Introduction.** With the goal of reducing reply on the ground tracking, the satellite autonomous navigation technologies are developed quickly in the recent several decades [1]. However, calculating a satellite orbit at high orbital altitudes is an important and challenging problem [2]. Basically, there are two kinds of individual autonomous orbits determination method depending on their measurement is angle to object such as star tracker or scalar to object such as GPS. Till now, most of the existing sensors are angle relied, which means it is more advantageous in attitude determination. GPS/GNSS becomes the vital option of autonomous navigation for space mission. And previous research demonstrated an approach to autonomous orbit estimation using onboard GPS receivers which are reliable and are utilized widely and routinely in satellite missions for orbit determination and control [3-5]. However, GPS based autonomous navigation for a satellite at high orbital altitude (>20000km) and beyond is more challenging than low earth orbits. The main reason is that high earth orbit is where acquisition of GPS signals is severely limited and the poor geometry.

XNAV, or X-ray pulsar navigation is an emerging concept for using X-ray pulsars which emit stable, and periodic signals comparable to atomic clocks in the X-ray band [6]. The position and time of vehicle could be determined by tracking and obtaining the phase measurements from several identified pulsars in X-ray astronomers. The positioning

accuracy is about 1km with respect to the solar system baracenter [7]. It could be utilized as a kind of "natural Global Positioning System (GPS)" for vehicle autonomous navigation anywhere in the solar system [8,9].

As X-ray navigation's potential capability in space navigation, Woodfork researched the use of X-ray pulsars for aiding GPS satellite orbit determination in his master thesis [10]. His research aiming at improving the accuracy and robustness of the GPS satellites and clock estimation indicates the XNAV autonomously ability for high earth orbit satellites. With current technology the measuring frequency could not achieve the same level as GPS/GNSS because the natural weak pulsar X-ray radiation requires longer time of signal integration. Reversely, the GPS/GNSS has high frequency outputs but lacks signals when it is applied to high altitude earth orbits. Based on the above consideration, the deficiencies of applying GPS/GNSS on high altitude orbits can be developed by adding X-ray pulsar measurements. In our previous research, Li demonstrated the navigation performance can be developed by an integration using X-ray navigation and UV star and earth sensors in [11,12], and the performance of GEO satellite autonomous navigation with multi-GNSS systems in [13].

This paper has presented an algorithm for high earth orbit satellite autonomous navigation using XNAV and GNSS. Since Kalman filer is a well known approach to dealing with stochastic estimation [14] and two observation systems need to be taken account into information fusion, the overall algorithm is structured by a federal Kalman filter which contains three parts: 1) State equation: establish a satellite dynamics model for GEO satellite which prorogates orbital parameter; 2) Observation equations: XNAV observation system and GNSS observation system. X-ray phase measurements and GNSS pseudo-ranges are their observations respectively. XNAV and GNSS are considered as two terminal navigation sensors; 3) Data fusion: each observation equation and satellite orbital dynamics form a subsystem. Use Kalman filter scheme in a federated configuration to incorporate the two sensors data. In this study, GEO (geosynchronous orbit) satellite is adopted as the test satellites to examine the performance of the proposed algorithm. The numerical simulation shows that the federal Kalman filter blends the tow observation effectively, and therefore provides accurate orbit estimation results. The navigation performances using the proposed method are shown in the simulation results. The paper is organized as follows. In Section 2, the orbit dynamics and observation modeling are described. The orbit estimation algorithms using Kalman filter in federated configuration are derived in Section 3. Numerical simulation to verify the proposed algorithm is shown in Section 4. Finally, conclusions are presented in Section 5.

2. Satellite Dynamics and Observation Modeling.

2.1. Satellite dynamics.

In this section, the GEO satellite orbit dynamics is presented. As reference system, orbit dynamic system is normally embedded to the onboard GNSS system offering a referenced orbital element with high frequency for satellite. For this reason, the reference system is the foundation of whole navigation system. In a general form, the dynamical equation of the satellite state within the J2000.0 Earth Centered Inertial (ECI) coordinate system can be presented as,

$$\dot{\boldsymbol{X}}_{orbit} = f_{orbit}(\boldsymbol{X}_{orbit}, t) + \boldsymbol{W}_{orbit}(t) \tag{1}$$

where the states $\boldsymbol{X}_{orbit} = [x, y, z, v_x, v_y, v_z]^T$ are the position and velocity of the satellite, f_{orbit} is the function that describes the satellite state dynamics, and $\boldsymbol{W}_{orbit}(t)$ is the process noise of the state equation.

For a GEO satellite whose orbit height is about 36000km, the two-body acceleration effect, the non-spherical Earth gravitational potential effect, and the third body gravitational effects from the Sun and the Moon are needed to describe the satellite acceleration. Thus, the f_{orbit} can be written as,

$$
f_{orbit}(\boldsymbol{X}_{orbit}, t) =
$$

$$
\begin{bmatrix}
v_x \\
v_y \\
v_z \\
\frac{-\mu_e x}{r^3}\left[1 + J_2\left(\frac{R_e}{r}\right)^2 \frac{3}{2}\left(1 - 5\frac{Z^2}{r^2}\right) + J_3\left(\frac{R_e}{r}\right)^3 \frac{5}{2}\left(3 - 7\frac{Z^2}{r^2}\right)\frac{Z}{r} - J_4\left(\frac{R_e}{r}\right)^4 \frac{5}{8}\left(3 - 42\frac{Z^2}{r^2} + 63\frac{Z^4}{r^4}\right)\right] \\
+\mu_s\left(\frac{x_s - x}{|\mathbf{r}_s - \mathbf{r}|^3} - \frac{x_s}{|\mathbf{r}_s|^3}\right) + \mu_m\left(\frac{x_m - x}{|\mathbf{r}_m - \mathbf{r}|^3} - \frac{x_m}{|\mathbf{r}_m|^3}\right) \\
\frac{-\mu_e y}{r^3}\left[1 + J_2\left(\frac{R_e}{r}\right)^2 \frac{3}{2}\left(1 - 5\frac{Z^2}{r^2}\right) + J_3\left(\frac{R_e}{r}\right)^3 \frac{5}{2}\left(3 - 7\frac{Z^2}{r^2}\right)\frac{Z}{r} - J_4\left(\frac{R_e}{r}\right)^4 \frac{5}{8}\left(3 - 42\frac{Z^2}{r^2} + 63\frac{Z^4}{r^4}\right)\right] \\
+\mu_s\left(\frac{y_s - y}{|\mathbf{r}_s - \mathbf{r}|^3} - \frac{y_s}{|\mathbf{r}_s|^3}\right) + \mu_m\left(\frac{y_m - y}{|\mathbf{r}_m - \mathbf{r}|^3} - \frac{y_m}{|\mathbf{r}_m|^3}\right) \\
\frac{-\mu_e z}{r^3}\left[1 + J_2\left(\frac{R_e}{r}\right)^2 \frac{3}{2}\left(3 - 5\frac{Z^2}{r^2}\right) + J_3\left(\frac{R_e}{r}\right)^3 \frac{5}{2}\left(6 - 7\frac{Z^2}{r^2}\right)\frac{Z}{r}\right] + \frac{\mu_e}{r^2} J_3\left(\frac{R_e}{r}\right)^2 \frac{3}{2} \\
-J_4\left(\frac{R_e}{r}\right)^4 \frac{5}{8}\left(15 - 70\frac{Z^2}{r^2} + 63\frac{Z^4}{r^4}\right) + \mu_s\left(\frac{z_s - z}{|\mathbf{r}_s - \mathbf{r}|^3} - \frac{z_s}{|\mathbf{r}_s|^3}\right) + \mu_m\left(\frac{z_m - z}{|\mathbf{r}_m - \mathbf{r}|^3} - \frac{z_m}{|\mathbf{r}_m|^3}\right)
\end{bmatrix}
$$

where $r = \sqrt{x^2 + y^2 + z^2}$, the distance between center of Earth and user satellite; R_e, the Earth mean radius, WGS-84 reference frame; μ_e, the gravitational parameter of the Earth; J_2, J_3, J_4, the coefficients referred to the zonal harmonics and the terrestrial model; μ_s, μ_m, the gravitational parameters of the Sun and the Moon; $\mathbf{r}_s = [x_s, y_s, z_s]^T$; $\mathbf{r}_m = [x_m, y_m, z_m]^T$, the position vectors of the Sun and the Moon.

Other perturbations (such as atmospheric drag, solar radiation and Earth tidal) are negligible compared with the remaining effects in W_{orbit}. In most space mission, the satellite dynamics models are designed inside the navigation platform.

2.2. **XNAV observation model.** In this section, the observation model of the XNAV system using pulse phase information is presented. Range measurements along the line-of-sight to a pulsar from SSB can be computed by comparing a measured pulse TOA at the satellite with the predicted pulse TOA at the SSB origin. Using this difference in arrival times of several pulsars, the position of the satellite can be determined.

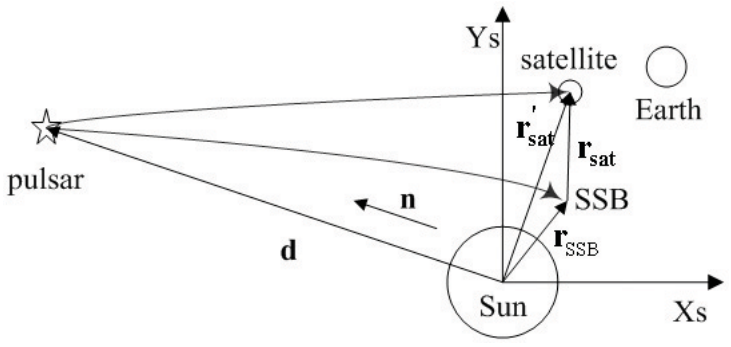

FIGURE 1. X-ray pulse from pulsar to the solar system

Figure 1 is a diagram of the pulse path from the pulsar to the solar system through the curved space-time. The positions of the pulsar, $\boldsymbol{d}$, the satellite, $\mathbf{r}_{sat}$, and the SSB, $\mathbf{r}_{SSB}$, with respect to the center of the Sun, are shown, as well as the satellite position with respect to the SSB, $\mathbf{r}_{sat}$, and the unit vector to the pulsar, $\mathbf{n}$. Since the Sun's gravitational

field can be considered symmetric about the z-axis, the pulse of photons arriving into the solar system will travel primarily in the x-y plane.

$$t_{SSB} - t_{sat} = \frac{\mathbf{n} \cdot \mathbf{r}_{sat}}{c} + t_{rel} \tag{2}$$

Equation (2) presents the basic relationship of the satellite position with respect to the SSB and the pulse TOA difference between the satellite and the SSB. Similar to GPS carrier phase measurements, the periodic signal introduces a phase ambiguity to the TOA difference measurements between the satellite and the SSB. Due to the inherent periodicity of the pulsars used in XNAV system, the TOA difference can be completed by estimating the phase of the pulsar based on a known pulse timing model. Assuming the integral ambiguity is $\triangle N$, Equation (2) can be represented with the pulse phase observed at the satellite ϕ_{sat}, and predicted at the SSB, ϕ_{SSB}, as

$$t_{SSB} - t_{sat} = [(\phi_{SSB} - \phi_{sat}) + \triangle N] \cdot P_{Pulsar} \tag{3}$$

P_{Pulsar} is the period of the pulsar. According to Equations (2) and (3), the TOA difference between the satellite and the SSB can be rewritten as,

$$[(\phi_{SSB} - \phi_{sat}) + \triangle N] \cdot P_{Pulsar} = \mathbf{n} \cdot \mathbf{r}_{sat}/c + t_{rel} \tag{4}$$

$\mathbf{r}_{sat}$ and $\mathbf{r}_E$ are the positions of satellite and Earth with respect to the SSB respectively, and $\mathbf{r}$ is the satellite position with respect to the Earth. As the satellite position vector $\mathbf{r}_{sat}$=$\mathbf{r}_E$ +$\mathbf{r}$. Equation (5) can be rewritten as,

$$[(\triangle\phi + \triangle N) \cdot P_{Pulsar} - t_{rel}] \cdot c - \boldsymbol{n} \cdot \boldsymbol{r}_E = \boldsymbol{n} \cdot \boldsymbol{r} \quad (\triangle\phi = \phi_{SSB} - \phi_{sat}) \tag{5}$$

where

$$\begin{aligned} \tilde{t}_{rel} = & \frac{1}{2cd_0}\left[(\boldsymbol{n} \cdot (\boldsymbol{r}_E + \tilde{\boldsymbol{r}}))^2 - \|\boldsymbol{r}_E + \tilde{\boldsymbol{r}}\|^2\right] \\ & + \frac{1}{cd_0}\left[(\boldsymbol{n} \cdot \boldsymbol{r}_{SSB})(\boldsymbol{n} \cdot (\boldsymbol{r}_E + \tilde{\boldsymbol{r}})) - (\boldsymbol{r}_{SSB}) \cdot (\boldsymbol{r}_E + \tilde{\boldsymbol{r}})\right] \end{aligned} \tag{6}$$

The Earth position $\boldsymbol{r}_E$ can be provided by JPL ephemeris data. The integral ambiguity of the pulsar can be calculated directly using satellite estimated position $\tilde{\boldsymbol{r}}$ as,

$$\triangle N = round\left(\boldsymbol{n} \cdot (\boldsymbol{r}_E + \tilde{\boldsymbol{r}})/\lambda + \tilde{t}_{rel}/D_p - \triangle\phi\right) \tag{7}$$

The function $round(x)$ rounds x to the nearest integer. When j pulsars are detected, the measure equations are as follows

$$\begin{bmatrix} ((\triangle\phi_1 + \triangle N_1) \cdot P_{P1} - \tilde{t}_{rel1}) \cdot c - \boldsymbol{n}_1 \cdot \boldsymbol{r}_E \\ ((\triangle\phi_2 + \triangle N_2) \cdot P_{P2} - \tilde{t}_{rel2}) \cdot c - \boldsymbol{n}_2 \cdot \boldsymbol{r}_E \\ \cdots \\ ((\triangle\phi_j + \triangle N_j) \cdot P_{Pj} - \tilde{t}_{relj}) \cdot c - \boldsymbol{n}_j \cdot \boldsymbol{r}_E \end{bmatrix} = \begin{bmatrix} \boldsymbol{n}_1{}^T & \boldsymbol{0}_{1\times3} \\ \boldsymbol{n}_2{}^T & \boldsymbol{0}_{1\times3} \\ \cdots & \\ \boldsymbol{n}_j{}^T & \boldsymbol{0}_{1\times3} \end{bmatrix} \cdot \begin{bmatrix} \boldsymbol{r} \\ \boldsymbol{v} \end{bmatrix} + \boldsymbol{V}(t) \tag{8}$$

where $\boldsymbol{r}$ is the position of the satellite; $\boldsymbol{v}$ is the velocity. P_{Pj} is the period of the j^{th} Pulsar. $\boldsymbol{V}(t)$ is the measuring noise. A simpler form of Equation (8) could be written as

$$\boldsymbol{Z}_{pulsar} = \boldsymbol{H}_{pulsar} \cdot \boldsymbol{X} + \boldsymbol{V}_{pulsar}(t) \tag{9}$$

2.3. **GNSS observation model.** In this section, the measurement model of the GNSS system using pseudo-range is presented. The difference in the reception of GNSS signals by satellite-borne receivers (in comparison to Low Earth Orbits Satellites) lies in the geometric distance between a GNSS satellite and the navigating satellite at high attitudes, where the GNSS satellite emits signals towards the Earth. Satellites at GEO, orbits are above the altitudes of the GNSS satellites, and reception of the signals is only possible from GNSS satellites at the other side of the Earth (see Figure 2). An extension of this

technique to geostationary (GEO) missions has been constrained by the difficulty of using GPS receivers due to poor GPS satellite visibility and weak signal power.

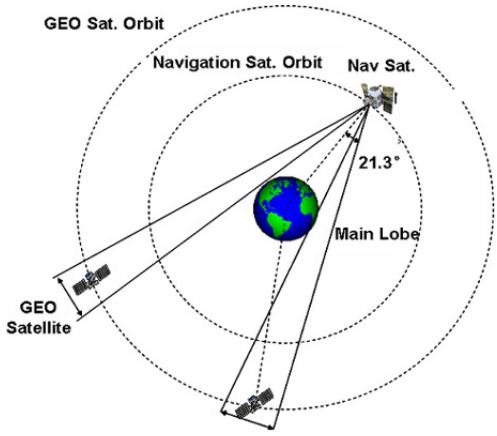

FIGURE 2. Satellite orbital geometry with respect to GNSS broadcast signal

These measurements are related to the satellite centre as the receiver location is assumed to be with respect to the satellite centre of mass in the satellite body-fixed frame. The measurement equation at each measurement time is:

$$\rho_j = r_j + \delta t_u + \nu_{\rho j} \tag{10}$$

where j, GNSS satellite index; ρ_j, the pseudorange form the user satellite to the navigation satellite S^j; $r_j = \sqrt{(x - x_{Sj})^2 + (y - y_{Sj})^2 + (z - z_{Sj})^2}$, the geometrical distance form the user satellite to the navigation satellite S^j; $\nu_{\rho j}$, the random measurement noise; δt_u, the range error equivalent to the receiver clock offset with respect to GNSS time.

When n satellites are available, the filter measure model can be expressed as:

$$\begin{bmatrix} \rho_1 \\ \rho_2 \\ \vdots \\ \rho_j \end{bmatrix} = \begin{bmatrix} \sqrt{(x - x_{N1})^2 + (y - y_{N1})^2 + (z - z_{N1})^2} + \delta t_u \\ \sqrt{(x - x_{N2})^2 + (y - y_{N2})^2 + (z - z_{N2})^2} + \delta t_u \\ \vdots \\ \sqrt{(x - x_{NJ})^2 + (y - y_{NJ})^2 + (z - z_{NJ})^2} + \delta t_u \end{bmatrix} + \begin{bmatrix} \nu_{\rho 1} \\ \nu_{\rho 2} \\ \vdots \\ \nu_{\rho j} \end{bmatrix} \tag{11}$$

A simpler form of Equation (11) could be written as

$$\boldsymbol{Z}_{GNSS} = \boldsymbol{h}_{GNSS}(X) + \boldsymbol{V}_{GNSS} \tag{12}$$

$\boldsymbol{V}_{GNSS}$, the receiver noise and all the measurement perturbations not included in the model are considered as Gaussian errors. $\boldsymbol{Z}_{GNSS}$ is a $j \times 1$ vector where j is the number of available GNSS signals. When j is greater than 4, the algorithm will select the best 4 according their geometry.

Different form XNAV system, in GNSS system there are another 2 states besides the orbit states. As this reason, the receiver clock is modeled too. The state of clock part X_{clock} is composed of clock bias and bias rates, i.e., $X_{clock} = [\ \delta t_u \quad \delta t_{ru}\ ]^T$. An exponentially correlated clock model driven by a zero mean white noise is integrated in the process model; refer as first order Markov processes. Here assumes the four different systems unified the time, so the clock error could be written as follows, and the parameter T_{ru} is the clock model correlation time.

$$\dot{X}_{clock} = f_{clock}(X_{orbit}, t) + W_{clock} = [\ \delta t_u \quad -\tfrac{1}{T_{ru}}\delta t_{ru}\ ]^T + [\ \omega_{tu} \quad \omega_{tu}\ ]^T \tag{13}$$

The resulting navigation state is an eight-state vector composed of six spacecraft position and velocity components and receiver clock bias, bias rates. For this reason the subsystem 1 extended its states to 8.

3. **Federal Filter Algorithm Structure.** The dynamical equation of satellite state is presented in Section 2.1, and the measurement models of the X-ray system and the GNSS based satellite navigation system are described in Sections 2.2 and 2.3. The model of the X-ray system is established as sub system 1 with Equation (1) and Equation (9). The model of the GNSS system is established as sub system 2 with Equation (1) and Equation (12).

The federated filtering technique is chosen to process data from these two systems [15]. The discrete form of these two subsystems can be presented as

$$I \begin{cases} \boldsymbol{X}(k+1) = f[\boldsymbol{X}(k)] + \boldsymbol{W}(k) \\ \boldsymbol{Z}_1(k) = H_1[\boldsymbol{X}(k)] + \boldsymbol{V}_1(k) \end{cases} \tag{14}$$

$$II \begin{cases} \boldsymbol{X}(k+1) = f[\boldsymbol{X}(k)] + \boldsymbol{W}(k) \\ \boldsymbol{Z}_2(k) = H_2[\boldsymbol{X}(k)] + \boldsymbol{V}_2(k) \end{cases} \tag{15}$$

The process noise of the state equation is $\boldsymbol{W}(k)$, and the measurement noises of the two subsystems, $\boldsymbol{V}_1(k)$ and $\boldsymbol{V}_2(k)$, can be supposed as the Gauss white noise. The covariance matrixes of these noises can be presented as

$$\begin{cases} E\left[\boldsymbol{W}(j) \cdot \boldsymbol{W}(k)^T\right] = \boldsymbol{Q}(k)\delta_{jk} \\ E\left[\nu_1(j) \cdot \nu_1(k)^T\right] = \boldsymbol{R}_1(k+1)\delta_{jk} \\ E\left[\nu_2(j) \cdot \nu_2(k)^T\right] = \boldsymbol{R}_2(k+1)\delta_{jk} \end{cases} \tag{16}$$

And the Kronecker Delta function δ_{jk} can be presented as

$$\delta_{jk} = \begin{cases} 1 & j = k \\ 0 & j \neq k \end{cases} \tag{17}$$

The structure of the federated filter is shown in Figure 3. Both β_1 and β_2 are the information sharing factors. The master filter does not perform filtering operation, only combining the outputs from two subsystems. Thus the information shared to the master filter is zero. According to the information-sharing principle, the information sharing factors must satisfy the following relationship:

$$\beta_1 + \beta_2 = 1 \tag{18}$$

Here the two factors are chosen as $\beta_1 = \beta_2 = 0.5$.

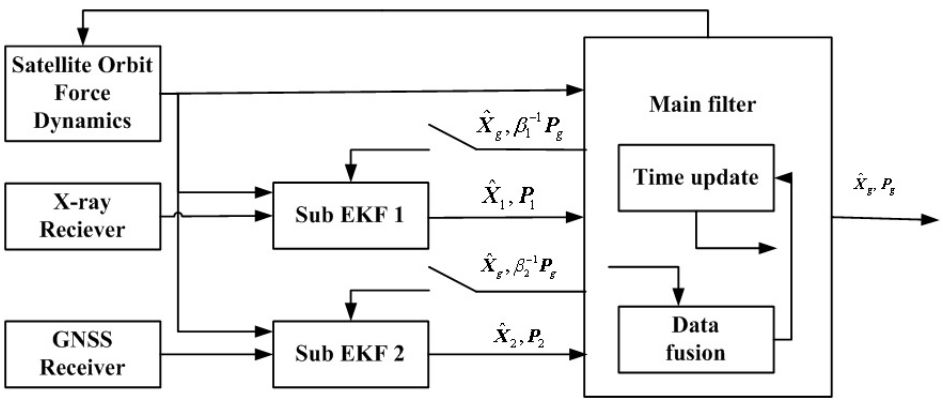

FIGURE 3. Structure of federal Kalman filter

For the i^{th} ($i = 1$ or 2) subsystem, local estimation of the subsystem is given as

$$\begin{cases} \hat{\mathbf{X}}_i(k) = \hat{\mathbf{X}}_g(k) \\ \mathbf{P}_i(k) = \beta_i^{-1}\mathbf{P}_g(k) \\ \mathbf{Q}_i = \beta_i^{-1}\mathbf{Q} \end{cases} \tag{19}$$

The local prediction and filtering equations of the i^{th} ($i = 1, 2$) subsystem using EKF can be written as follows [16]:

$$\hat{\boldsymbol{X}}_i(k+1/k) = \hat{\boldsymbol{X}}_i(k/k) + f[\boldsymbol{X}_i(k)] \cdot T \tag{20}$$

$$\hat{\boldsymbol{X}}_i(k+1) = \hat{\boldsymbol{X}}_i(k+1/k) + \delta\hat{\boldsymbol{X}}_i(k+1) \tag{21}$$

$$\delta\hat{\boldsymbol{X}}_i(k+1) = \boldsymbol{K}_i(k+1)\left\{\boldsymbol{Z}_i(k+1) - \boldsymbol{H}_i\left[\hat{\boldsymbol{X}}_i(k+1/k)\right]\right\} \tag{22}$$

$$\boldsymbol{P}_i(k+1/k) = \Phi_i(k+1/k)\boldsymbol{P}_i(k/k)\Phi_i(k+1/k)^T + \mathbf{Q}_i \tag{23}$$

$$\begin{aligned} \boldsymbol{K}_i(k+1) = {} & \boldsymbol{P}_i(k+1/k)\boldsymbol{H}_i(k+1)^T[\boldsymbol{H}_i(k+1) \\ & \times\boldsymbol{P}_i(k+1/k)\boldsymbol{H}_i(k+1)^T + \boldsymbol{R}_i(k+1)]^{-1} \end{aligned} \tag{24}$$

$$\begin{aligned} \boldsymbol{P}_i(k+1) = {} & [\boldsymbol{I} - \boldsymbol{K}_i(k+1)\boldsymbol{H}_i(k+1)]\boldsymbol{P}_i(k+1/k)[\boldsymbol{I} - \boldsymbol{K}_i(k+1) \\ & \times\boldsymbol{H}_i(k+1)]^T + \boldsymbol{K}_i(k+1)\boldsymbol{R}_i(k+1)\boldsymbol{K}_i(k+1)^T \end{aligned} \tag{25}$$

where $\boldsymbol{P}$ is the covariance matrix of the state estimation uncertainty, $\boldsymbol{K}$ is the Kalman gain matrix, Φ is the state transition matrix of the discrete dynamic system, and $\boldsymbol{T}$ is integration interval of the filter.

With the outputs from two subsystems, the output of the master filter can be presented as

$$\begin{cases} \hat{\mathbf{X}}_g = \mathbf{P}_g\left(\mathbf{P}_1^{-1}\hat{\mathbf{X}}_1 + \mathbf{P}_2^{-1}\hat{\mathbf{X}}_2\right) \\ \mathbf{P}_g = (\mathbf{P}_1^{-1} + \mathbf{P}_2^{-1})^{-1} \end{cases} \tag{26}$$

Given the initial state estimation $\hat{\mathbf{X}}_g(0)$, the covariance estimation $\mathbf{P}_g(0)$, and the process noise matrix Q, the information is shared to two subsystems by (19). The subsystem processes the data using EKF from (20) to (25), and the optimal estimation of the state is derived by infusing the outputs from two subsystems with (26).

4. **Simulation.**

The orbit determination system has been described in the previous section. In this section, the performance of the system is analyzed using a Monte-Carlo simulation.

4.1. **Simulation description.**

4.1.1. *Scenario setting.* The test simulations elapse 24 hours. The scenario epoch starts at 30 April 2009 12:00:00.00 UTCG, stops at 1 May 2009 12:00:00 UTCG.

TABLE 1. Force model setting for satellite

Mass of satellite	$1000kg$	Ineria Matrix	$diag[3.35kg \cdot m^2\ 11.37kg \cdot m^2\ 8.08kg \cdot m^2]$		
Earth Gravity model	WGS84 EGN96	Maximum Degree	21	Maximum order	21
Solar Radiation Pressure (SRP) model	Spherical	Cr	1.0	Area/Mass Ratio for SRP	$0.02m^2/kg$
Atomosphere density model for drag	*Jacchia-Roberts*	Cd	2.2	Area/Mass Ratio for drag	$0.02m^2/kg$
Third body gravity use		*Sun and Moon*			
Solar Flux/GeoMag		Daily F10.7	150	Average F10.7	150
		Geomagnetic Index(Kp)		3.0	

4.1.2. *Orbit propagation.* The nominal orbital data in J2000 Geocentric inertial coordinate is generated by STK (satellite tool kit) software. The HPOP mechanical model is used to simulate the real force motion of the satellite where non-spherical gravitation perturbation, the solar and sun perturbation, the sunlight pressure and the atmospheric perturbation are considered. Force model for satellite setting are shown in Table 1.

HPOP Integrator for test satellites is Runge-Kutta Fehlberg integration method of 7^{th} order with 8^{th} order error control for the integration step size which is 1 second. The output frequency of orbit propagation is 1s. The GEO satellite was modeled as an earth-pointing geostational satellite, and its elements see Table 2.

TABLE 2. User orbital elements

Orbittype		Geostationary	
Cartesian(J2000)		Keplerian(J2000)	
$X(m)$	–26,214,220,335.009	Semi-major Axis(m)	42,164,169.637
$Y(m)$	33,024,715,796.160	Eccentricity	1.42579e-15
$Z(m)$	0	$Inclination(^\circ)$	0
$V_x(m/s)$	–2,408.201	$RAAN(^\circ)$	0
$V_y(m/s)$	–1,911.571	$Lon.Ascn.Node(^\circ)$	90
$V_z(m/s)$	0.000	$TrueAnomaly(^\circ)$	128.441696

4.1.3. *Pulsar selection.* In X-ray Navigation subsystem, PSR B0531+21, PSR B1937+21, PSR B1821-24, PSR B1957+20 these four pulsars are used in the simulation. The distance precision in the line of sight of the 4 pulsars are 109m, 344m, 325m and 1866m, respectively. The update cycle of the X-ray Navigation is 500s, as the Signal-to-Noise of X-ray pulsar radiation is lower and needs hundreds seconds to form a clear profile. Define Single-XNAV means only using PSR B0531+21, while Multi-X-ray pulsar means using PSR B0531+21, PSR B1937+21, PSR B1821-24 and PSR B1957+20.

4.1.4. *GNSS simulation.* Since there are four GNSS constellations, here the multi-GNSS are assumed which consists of the current 31 GPS satellites, assumed 24 GLONASS satellites, planned 30 GALILEO satellites and possible 27 COMPASS satellites [17,18]. The STK software (www.stk.com) is used to establish the GNSS Satellite Database.

GNSS receiver has a down-looking antenna to the Earth. Here the impact of the weak signal tracking capabilities is not discussed. Satellites are considered as visible and available if its line of sight is inside the transmission cone and inside the reception cone, and does not cross the Earth. The antenna half-cone is set as follows: Navigation satellite transmit antenna half-cone angle: 21.3° which means receive main lobe is only considered. User satellite receiver antenna half-cone angel is 90°. Define Single-GNSS means using BEIDOU navigation constellation, while Multi-GNSS means using GPS, GLONASS, BEIDOU and GALILEO.

Initial parameters for Kalman filter in GNSS navigation subsystem, the pseudo range measurement noise is 5m. The noises of the GNSS clock and frequency difference are 0.1m and 0.001m. The update cycle of the GNSS is 5s.

The covariance matrix of process noise W_{orbit} is,

$$Q = diag\big(\big[(0.35m)^2, (0.35m)^2, (0.35m)^2, (3.5\times10^{-4}m/s)^2, (3.5\times10^{-4}m/s)^2, (3.5\times10^{-4}m/s)^2\big]\big)$$

The initial errors of the satellite position and velocity are,

$$\delta X(0) = [3km, 3km, 3km, 1m/s, 1m/s, 1m/s]$$

The initial covariance matrix of the satellite position and velocity is given as

$$P_g(0) = diag\left(\left[(3km)^2, (3km)^2, (3km)^2, (1m/s)^2, (1m/s)^2, (1m/s)^2\right]\right)$$

The errors of position and velocity are defined as

$$\delta r = \sqrt{(\hat{x}-x)^2 + (\hat{y}-y)^2 + (\hat{z}-z)^2}$$

$$\delta \nu = \sqrt{(\hat{\upsilon}_x - \nu_x)^2 + (\hat{\nu}_y - \nu_y)^2 + (\hat{\nu}_z - \nu_z)^2}$$

where x, y, z, ν_x, ν_y, ν_z are the true value of the satellite position and velocity, and $\hat{x}$, $\hat{y}$, $\hat{z}$, $\hat{\nu_x}$, $\hat{\nu_y}$, $\hat{\nu_z}$ are the estimated values of them. If the value of the position error δr is recorded for different samples $(\delta r_1, \delta r_2, \cdots, \delta r_N)$, then the root mean square (RMS) of δr is defined as

$$RMS(\delta r) = \sqrt{E(\delta r^2)} \cong \sqrt{\frac{1}{N}\sum_{i=1}^{N} \delta r_i^2}.$$

The RMS of $\delta\nu$ can also be defined as

$$RMS(\delta \nu) = \sqrt{E(\delta \nu^2)} \cong \sqrt{\frac{1}{N}\sum_{i=1}^{N} \delta \nu_i^2}.$$

4.1.5. *Integration mode.* According to the number of pulsars measurement and the number of GNSS system used, there are four integration modes, as follows:

Mode 1: Single-GNSS +Single-XNAV Mode 2: Multi-GNSS +Single-XNAV
Mode 3: Single-GNSS +Multi-XNAV Mode 4: Multi-GNSS +Multi-XNAV

4.2. **Simulation results.** Figure 4 and Figure 5 are the navigation performance of Single GNSS and Multi GNSS, show the estimation error curves and the covariance curves. The filter results rebound in Figure 4 as the number of visible satellites reduces, i.e., the number of visible navigation satellites is less than four which verify the sensitivity of Kalman filter based GNSS navigation performance to the visible navigation satellites accordingly the filter results has better convergent because the EKF in subsystem 2 has more measures.

The navigation accuracy of Single GNSS and Multi GNSS are 99.947m and 69.918m respectively. Besides, our previous research test that single X-ray and multi XNAV have around 600m and 100m accuracy respectively [19].

Figure 6 to Figure 9 are filter results of the position and velocity in four integration mode as defined and the position and velocity estimation errors are collected in Table 3 accordingly. These results indicate that 1) the covariance of the estimate errors is convergent during the elapsed hours, which means the federal EKF is contributing in all the four working mode; 2) Because the integration of XNAV and GNSS systems, the precision of navigation is improved to a level less than 100m navigation accuracy; 3) Integrated with Multi GNSS system (Figure 7 and Figure 9) produced significantly small

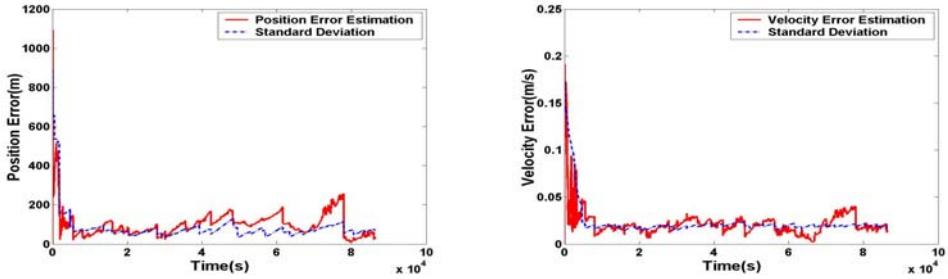

(a) Position error estimation (b) Velocity error estimation

FIGURE 4. Single GNSS navigation performance

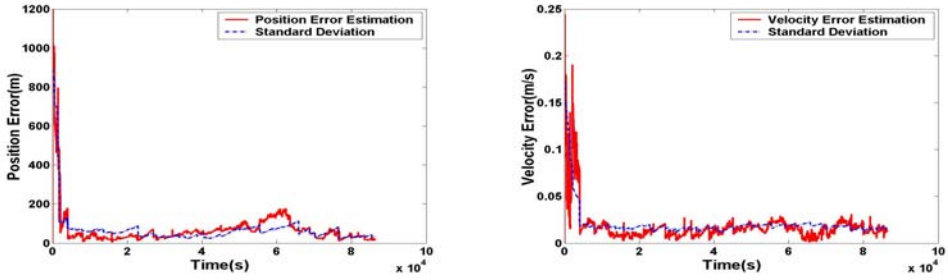

(a) Position error estimation (b) Velocity error estimation

FIGURE 5. Multi GNSS navigation performance

errors for the reason that GNSS is a manmade system with fast frequency and qualified outputs. Hence, Mode 3 (Figure 8) and Mode 1 (Figure 6) have poorer solution than Mode 4 and Mode 2.

TABLE 3. The 90° GEO Filtering accuracy in different integrated mode

Integrated mode	Position estimation errors (m)	Velocity estimation errors (m/s)
Single GNSS	99.947	0.021
Multi GNSS	69.918	0.0173
Mode 1 Single-GNSS + Single-XNAV	71.366	0.017
Mode 2 Multi-GNSS + Single-XNAV	41.319	0.012
Mode 3 Single-GNSS + Multi-XNAV	66.970	0.017
Mode 4 Multi-GNSS + Multi-XNAV	40.286	0.013

In addition, for some reason such as GPS are controlled by the US Military, multi GNSS has more challenge to realize. Therefore, satellite autonomous navigation could only utilize single GNSS. In this situation, it is optimized to adding single GNSS with reliable, celestial body based XNAV. With currently technology, the deficiency of XNAV is it requires longer signal integration times to produce an acceptable signal-to-noise ratio forming a pulsar wave profile. However, as a terminal navigation sensor, XNAV's performance such as output frequency could be improved in the future. However, Mode 3 and Mode 1 have better solution than Single GNSS mode. And if Multi-XNAV is adopted, its navigation accuracy is equivalent to Multi-GNSS mode.

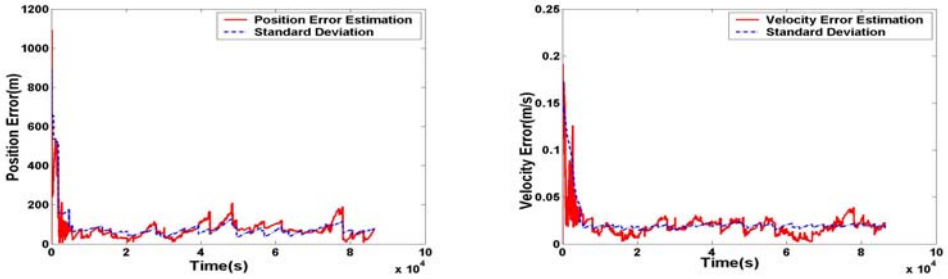

(a) Position error estimation (b) Velocity error estimation

FIGURE 6. SGNSS+SXNAV navigation performance

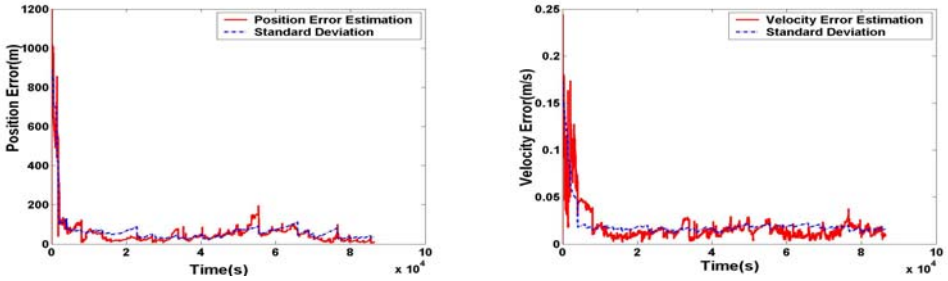

(a) Position error estimation (b) Velocity error estimation

FIGURE 7. MGNSS+SXNAV navigation performance

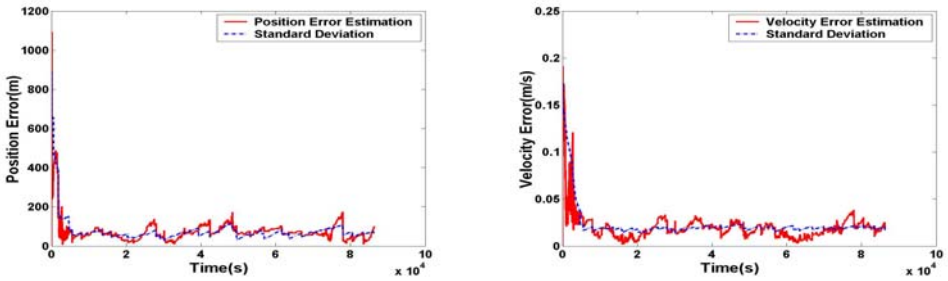

(a) Position error estimation (b) Velocity error estimation

FIGURE 8. SGNSS+MXNAV navigation performance

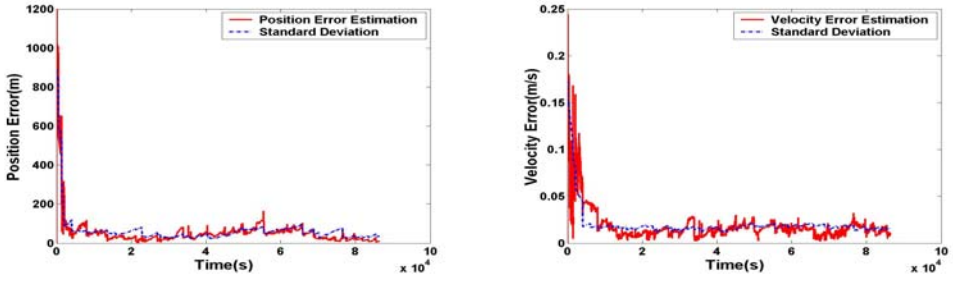

(a) Position error estimation (b) Velocity error estimation

FIGURE 9. MGNSS+MXNAV navigation performance

5. **Conclusions.** This paper is an attempt to investigate the navigation performance using federal extend Kalman filter in the hypothesis that X-ray Navigation and GNSS systems are worked. Generally, Satellite autonomous navigation accuracy is a function of the navigation algorithm and observation measurement type, quality and frequency. In this paper, the navigation algorithm is structured using federal Extend Kalman filter. The simulation results show it could well blend the XNAV and GNSS observations.

In fact, X-ray Navigation is considered as a backup of GNSS/GPS, as this navigation method can apply a fully navigation parameters including time, position and attitude like GNSS. The combination of these two navigation method can offer a better navigation performance in precision and reliability.

With this consideration, a GEO autonomous navigation algorithm using X-ray Navigation and GNSS measurements is developed in this paper. The simulation software is coded using STK and Matlab. The results of the four potential working modes validate that <100m navigation accuracy can be gained by integration, and these tow system can be back-up reciprocally. And in the real world, different work mode could be chosen according to practical condition.

The performance results presented in this paper are optimistic due to the simulation of measurements errors characteristic of an X-ray navigation sensor with a perfect timing system. And the time and coordinate systems transition between different GNSS systems are not considered in this article. Therefore, future direction will include a detailed investigation of the impact of using a satellite onboard timing system with actual errors.

Acknowledgment. This work was partially supported by the National Natural Science Foundation of China (Grant No. 91016019, 60904091), the National Program on Key Basic Research Project (973 Program) (2009CB724002), the Innovative Scientific Research Team Foundation of Jiangsu Province 2009, the Priority Academic Program Development of Jiangsu Higher Education Institutions, the Funding for Outstanding Doctoral Dissertation in NUAA (Grant No. BCXJ10-05), the Qing Lan Project of Jiangsu Province. The author would like to thank the anonymous reviewers for helpful comments and valuable remarks.

REFERENCES

[1] T. J. Alfred, Autonomous navigation, When will we have it? *Institute of Navigation, National Technical Meeting*, Anaheim, CA, USA, pp.96-105, 1987.

[2] W. Bamford, L. Winternitz and C. Hay, Innovation autonomous navigation at high earth orbits, *GPS World*, 2006.

[3] O. Balbach, B. Eissfeller, G. W. Hein, T. Zink et al., Tracking GPS above GPS satellite altitude: Results of the GPS experiment on the HEO mission equation, *IEEE Position Location and Navigation Symposium*, Palm Spring, CA, USA, pp.243-249, 1998.

[4] C. Altmayer, S. Martin and S. Theil, Autonomous onboard orbit and attitude control of geostationary satellites using pseudolites, *Proc. of ION GPS-98*, Nashvill, TN, USA, 1998.

[5] E. Gill, O. Montenbruck and K. Brieb, GPS-based autonomous navigation for the BIRD satellite, *International Symposium Space Flight Dynamics*, Biarritz, France, 2000.

[6] E. H. John, Principles of X-ray navigation, *Standford Linear Accelerator Center*, Standford University, 1996.

[7] S. I. Sheikh, *The Use of Variable Celestial X-ray Sources for Spacecraft Navigation*, Ph.D. Thesis, University of Maryland, 2005.

[8] P. Graven, J. Collins, S. Sheikh, J. Hanson, P. Ray and K. Wood, XNAV for deep space navigation, *The 31st Annual AAS Guidance and Control Conference, AAS 08-054*, 2008.

[9] P. Graven, J. Collins, S. Sheikh and J. Hanson, XNAV beyond the moon, *Proc. of the 63rd Annual Meeting of the Institute of Navigation*, pp.423-431, 2007.

[10] D. W. Woodfork, *The Use of X-ray Pulsars for Aiding GPS Satellite Orbit Determination*, Air Force Institute of Technology, Wright-Patterson Air Force Base, OH, USA, 2005.

[11] L. Qiao, J. Liu, G. Zheng and Z. Xiong, The algorithm and simulation for satellite navigation using X-ray pulsars, *Proc. of SPIE the 2nd International Conference on Space Information Technology*, vol.6795, pp.F7953-F7953, 2007.

[12] L. Qiao, J. Liu, G. Zheng and Z. Xiong, Augmentation of XNAV system to an ultraviolet, *2009 Sensor-Base Satellite Navigation System, IEEE Journal of Selected Topics in Signal Processing*, vol.3, no.5, pp.777-785, 2009.

[13] L. Qiao, S. Lim, C. Rizos and J. Liu, Autonomous GEO satellite navigation algorithm with multiple GNSS measurements, *The 22nd International Technical Meeting of the Satellite Division of the Institute of Navigation (ION GNSS)*, Savannah, GA, USA, 2009.

[14] A. Ohsumi, T. Kimura and M. Kono, Kalman filter-based identification of unknown exogenous input of stochastic linear systems via pseudomeasurement approach, *International Journal of Innovative Computing, Information and Control*, vol.5, no.1, pp.1-16, 2009.

[15] Y. Qing, H. Zhang and S. Wang, *Kalman Filter and Integrated Navigation Principle*, Northwest Polytechnical University Press, 2004.

[16] N. A. Carlson, Federated square root filter for decentralized parallel processors, *IEEE Trans. on Aero. and Elec.*, vol.26, no.3, pp.517-525, 1990.

[17] D. Svehla and M. Heinze, Positioning with the four GNSS: GPS, GLONASS, GALILEO and BEIDOU based on phase clocks, *European Geophysical Union, General Assembly Vienna*, 2007.

[18] S. Tan, Development and though of compass navigation satellite system, *Journal of Astronautics*, vol.29, no.2, pp.391-396, 2008.

[19] L. Qiao, *X-ray Pulsar-Based Autonomous Navigation and Its Application to High Earth Orbits Satellites*, Ph.D. Thesis, Nanjing University of Aeronautics and Astronautics, China, 2010.